LITERATURE CITED

Brodkey, R. S., K. N. McKelvey, H. C. Hershey, and S. G. Nychas, "Mass Transfer at the Wall as a Result of Coherent Structures in a Turbulently Flowing Liquid," *Int. J. Heat Mass Transfer*, **21**, 593 (1978).

Campbell, J. A., "The Use of a Regular Eddy Model to Describe Turbulent Mass Transfer to a Wall," M.S. Thesis, University of Illinois, Urbana (1979).

Campbell, J. A., "The Velocity-Concentration Relationship in Turbulent Mass Transfer to a Wall," Ph.D. Thesis, University of Illinois, Urbana (1981).

Campbell, J. A., and T. J. Hanratty, "Influence of Turbulent Structure on Mass Transfer at a Solid Surface," Proceedings of 2nd Symposium on Turbulent Shear Flows, London (1979).

Campbell, J. A., and T. J. Hanratty "Mass Transfer Between a Turbulent Fluid and a Solid Boundary: Linear Theory," *AIChE J.*, p. 988 (Nov., 1982).

Campbell, J. A. and T. J. Hanratty, "Turbulent Velocity Fluctuations that Control Mass Transfer to a Solid Boundary," *AIChE J.*, (March, 1983).

Eckelman, L. D., "The Structure of Wall Turbulence and its Relation to Eddy Transport," Ph.D. Thesis, University of Illinois, Urbana (1971).

Eckelmann, H., "The Structure of the Viscous Sublayer and the Adjacent Wall Region in Turbulent Channel Flow," *J. Fluid Mech.*, **65**, 439 (1974).

Fortuna, G., "The Effect of Drag-Reducing Polymers on Flow Near a Wall," Ph.D. Thesis, University of Illinois, Urbana (1970).

Hatziavramidis, D. T., and T. J. Hanratty, "The Representation of the Viscous Wall Region by a Regular Eddy Pattern," *J. Fluid Mech.*, **95**, 655 (1979).

Hogenes, J. H. A., "Identification of the Dominant Flow Structure in the Viscous Wall Region of a Turbulent Flow," Ph.D. Thesis, University of Illinois, Urbana (1979).

Laufer, J., "The Structure of Turbulence in Fully Developed Pipe Flow," *NACA TN 2954* (1953).

Lin, C. S., R. W. Moulton, and G. L. Putnam, "Mass Transfer Between Solid Wall and Fluid Streams," *Ind. Eng. Chem.*, **45**, 636 (1953).

Reiss, L. P., "Investigation of Turbulence Near a Pipe Wall Using a Diffusion Controlled Electrolytic Reaction on a Circular Electrode," Ph.D. Thesis, University of Illinois, Urbana (1962).

Roache, P. J., "Computational Fluid Dynamics," Hermosa Publishers, Albuquerque, N.M. (1972).

Shaw, D. A., "Mechanism of Turbulent Mass Transfer to a Pipe Wall at High Schmidt Number," Ph.D. Thesis, University of Illinois, Urbana (1976).

Shaw, D. A. and T. J. Hanratty, "Influence of Schmidt Number on the Fluctuations of Turbulent Mass Transfer to a Wall," *AIChE J.*, **23**, 160 (1977).

Sirkar, K. K., "Turbulence in the Immediate Vicinity of a Wall and Fully Developed Mass Transfer at High Schmidt Numbers," Ph.D. Thesis, University of Illinois, Urbana (1969).

Sirkar, K. K. and T. J. Hanratty, "Relation of Turbulent Mass Transfer at High Schmidt Numbers to the Velocity Field," *J. Fluid Mech.*, **44**, 589 (1970).

Van Shaw, P., "A Study of the Fluctuations and the Time Average of the Rate of Turbulent Mass Transfer to a Pipe Wall," Ph.D. Thesis, University of Illinois, Urbana (1963).

Manuscript received August 19, 1981; revision received April 7, and accepted April 19, 1982.

Experimental Measurements of the Effect of Viscosity on Drag for Liquid Drops

The drag coefficients of drops of various liquids falling in air were measured experimentally. The drag coefficient was linearly related to the viscosity in the Reynolds number and viscosity range measured. Measurements also suggested there is no difference between Newtonian and non-Newtonian liquids.

P. H. GILLASPY and T. E. HOFFER

Atmospheric Sciences Center
Desert Research Institute
University of Nevada System
Reno, NV 89506

SCOPE

Calculating fall trajectories and transport properties between a drop and its medium depends on a knowledge of the drag forces acting on the liquid drop. It has been found that the Reynolds number (Re) is the primary parameter characterizing the forces acting (Stokes, 1851; Reynolds, 1883). In the Stokes flow regime ($Re < 1$), exact solution of the Navier-Stokes equation for a sphere yields an expression for drag in excellent agreement with measurements for spheres and liquid drops. In the intermediate range ($1 < Re < 500$), numerical solutions (Hamielec et al., 1967; LeClair et al., 1970) give drag coefficients with excellent experimental agreement. The range of higher Re sees a whole host of experimental measurements for spheres and liquid drops with the main emphasis on water drops due to their relevance to atmospheric sciences. Although the manner in which the various forces act is well understood, previous studies have not been able to express quantitatively the effect of liquid viscosity or surface tension on the drag at higher Re.

In the analysis of experimentally measured drag coefficients reported in this paper, quantitative assessment of the role of liquid drop viscosity on the drag is presented. Non-Newtonian as well as Newtonian liquids were used to separate the possible effects of rheological properties.

CONCLUSIONS AND SIGNIFICANCE

Experimental measurements have been reported that show qualitatively and quantitatively the effects of liquid viscosity on the drag of liquid drops falling through air. The quantitative effects of viscosity have been shown to be modeled by a function of the form

$$C_D = C_D(Re,\mu = \infty)\left[1 - B\frac{\mu_a}{\mu} f(Re)\right] \qquad (1)$$

Correspondence concerning this paper should be addressed to P. H. Gillaspy at NASA/MSFC, Space Sciences Laboratory, ES-83, Huntsville, AL 35812.

0001-1541-83-6815-0229-$2.00.

valid at least for 800 ≤ Re ≤ 2,000 and $\mu \geq 3.0$ mPa·s(3.0 cp). In the limit of high Re, the internal circulation is limited by the drop distortion. The above expression described the non-Newtonian as well as Newtonian liquids used. These results represent a first step in the analysis of physical property effects on the drag of liquid drops.

THEORY

The measurements reported in this paper are presented in the form of data relating the coefficient of drag (C_D) to the Reynolds number (Re). Both of these quantities are derived from the actual parameters measured, fall velocity and drop mass. Therefore, it is appropriate to give a brief discussion describing the calculation of C_D and Re from the fall velocity and drop mass.

The resisting force exerted by a medium on a body passing through it is called the drag. Normally, the drag cannot be measured directly and, in fact, neither the shape nor pressure distribution are known quantities for deformable liquid drops. By physical reasoning the drag force (D) can be related to the dynamic pressure by

$$D = C_D 1/2 \rho_a V_T^2 \pi r^2. \tag{2}$$

For falling liquid drops, C_D can be calculated by measuring the fall velocity provided that the drop mass is known. In that instance, the analysis is as:

At terminal velocity, the drag will be balanced by gravity

$$D = mg = \frac{4}{3} r^3 (\rho_l - \rho_a) g. \tag{3}$$

From Eqs. 2 and 3, C_D becomes

$$C_D = \frac{8}{3}\left(\frac{\rho_l}{\rho_a} - 1\right)\frac{gr}{V_T^2}. \tag{4}$$

The drop radius is obtained by weighing the drop and calculating the equivalent spherical radius

$$r = \left(\frac{3m}{4\pi\rho_l}\right)^{1/3} \tag{5}$$

which is used in Eq. 4 even though the drop may be deformed from spherical.

The drag is intimately related to the flow pattern about the drop. When the Navier-Stokes equation for viscous incompressible flow is nondimensionalized, the dimensionless parameter governing the nature of the flow pattern (laminar or turbulent) is formed. This is the Reynolds number, Re. Re is the ratio of the dynamic pressure (inertial force) to the shearing stress (viscous force),

$$Re = \frac{2r\rho_a V_T}{\mu_a} = \frac{\rho_a V_T^2}{\left(\frac{\mu_a V_T}{2r}\right)}. \tag{6}$$

By suitable rearrangement of variables in Eq. 4, a relation between C_D and Re can be obtained as

$$V_T = \frac{16}{3} g(\rho_l - \rho_a)\frac{r^2}{\mu_a}\frac{1}{C_D Re} \tag{7}$$

Thus, the relation of C_D vs. Re forms a unique combination which determines the fall velocity of a drop. Drag measurements are usually presented showing values of C_D vs. Re for this reason among others. One can also show from dimensional analysis the following functional relation

$$f\left(\frac{2r\rho_a V}{\mu_a}, \frac{2D\rho_a}{\pi r^2 V^2 \mu_a}\right) = f(Re, C_D) = 0. \tag{8}$$

A liquid drop, unlike a solid sphere, can develop an internal circulation within it due to the shearing stress at the liquid-gas interface. It could be expected that the internal circulation can affect the drag significantly if of sufficient degree. The internal circulation itself is not evaluated but is related to drag via the ratio of the drop's fluid viscosity to that of air (Hadamard, 1911). This ratio determines the efficiency at which momentum is transported across the liquid-air interface. Some theoretical evaluations have been accomplished and can now be discussed, although it should be kept in mind that all determinations of drag at $Re \geq 500$ are experimental.

The drag coefficient is composed of two components, frictional (C_{DF}) and pressure (C_{DP}), which are given by LeClair et al. (1972) as

$$C_{DF} = \frac{8}{Re}\int_0^\pi \left[\left(\frac{\partial v}{\partial r} - \frac{v}{r}\right)\sin\theta - \frac{2\partial u}{\partial r}\cos\theta\right]\sin\theta d\theta \tag{9a}$$

$$C_{DP} = \int_0^\pi p(r = a, \theta)\sin 2\theta d\theta, \tag{9b}$$

$$C_D = C_{DF} + C_{DP}. \tag{9c}$$

LeClair et al. (1972) have numerically evaluated these expressions for water drops of $Re \leq 400$. The hope of evaluating the expressions for higher Re is quite dim owing to the complexity of interactions among several factors. The above expressions require a knowledge of the external aerodynamic pressure distribution as well as the internal circulation pattern. For a noncirculating drop, the aerodynamic pressure will be determined by shape and Re alone, but when internal circulation is in effect it alters not only the friction drag by decreasing the velocity shear at drop surface but also the pressure drag by retarding the separation of the boundary layer. Fortunately, it appears (Savic, 1950; McDonald, 1954; Pruppacher and Pitter, 1971; Green, 1975) that internal circulation generally has little effect on drop shape.

A mathematical expression for relating internal circulation to drag for Stokes flow of a liquid sphere has been found by Hadamard (1911) and Rybczinski (1911) as

$$C_D = C_{DS}\left(\frac{1 + 2/3\frac{\mu_a}{\mu}}{1 + \frac{\mu_a}{\mu}}\right) \tag{10}$$

$$C_D = C_{DS}\left(1 - \frac{1}{3}\frac{\mu_a}{\mu}\right): \quad \frac{\mu_a}{\mu} \ll 1. \tag{11}$$

The expression shows the drag to be linearly related to the internal circulation, but the effect is <1%. The measurements reported herein permit the derivation of an expression for Re above the Stokes flow regime.

EXPERIMENTAL APPARATUS

The experimental apparatus consists of the drop generator, fall column, timing equipment, electronic signal conditioning, and a microprocessor which allows the evaluation of data in real time.

The fall column, Figure 1, is constructed of several sections of 152-mm (6-in.) inner diameter PVC pipe. The column extends through three floors of the Atmospheric Sciences Center building giving a total usable fall distance of 11.36 m. The column is sealed to minimize air circulation created by pressure differentials between the third and first floors. In addition, those sections located on the first and second floors are enclosed and cooled by circulating air around the fall column. These measures isolated the column from the building's air-conditioning system and insured hydrostatic stability within the column.

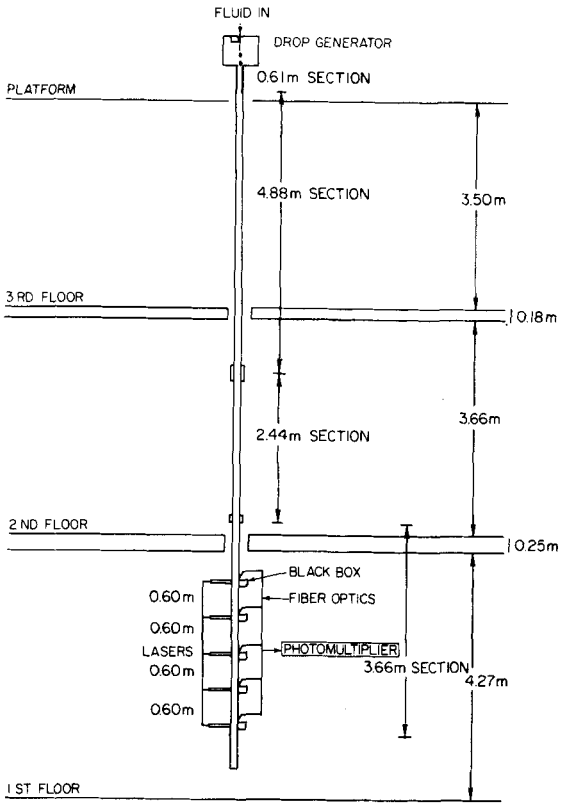

Figure 1. Fall column.

For measurements in the range $Re > 800$, drops are formed on the tip of glass or metal capillary tubing and allowed to detach and fall into the top of the column. For $Re = 100$–200, a vibrating needle technique (Eaton and Hoffer, 1970) is used. The drop generator enclosure mounts on a micrometer stage and connects to the column pipe through flexible neoprene tubing. By adjusting the micrometer, the drops could be positioned to fall within ± 1 mm of the center of the column. Due to the sensitivity of the large drops to the roughness of the tubing tip and the distortion and oscillation of the drops, very few of the drops fall along the vertical.

However, as will be discussed, this does not affect the data since the alignment of the lasers and fiber optics insured that only drops which fell vertically in the center of the column were measured. The drop production rate was always kept less than 1 every 5 s. Since it took a maximum of 3 s for the drops to traverse the column, any wake effect interaction between successive drops was negligible (Happel and Brenner, 1965; Eaton and Hoffer, 1970). The drop mass was determined by collecting a drop at the top of the column in a small aluminum foil cup and weighing the cup, whose weight is tared out, and drop on a Cahn 25 Electrobalance which resolves to 10 μg for drops of 10 mg (2,500-μm diameter). All liquids used had a vapor pressure typically a hundred times lower than water so that evaporation was <0.01%. Since it took only 15 s for the balance to settle, any error introduced by evaporation was insignificant. In actual measurements, the mass varied for a series of drops by about 1% for large drops (>20 mg) and <1% for smaller drops. The variation for non-Newtonian liquid drops was slightly greater than Newtonian because of the formation of a thin spider weblike filament that formed when non-Newtonian drops broke off from the tubing. This trailing filament broke off from the main drop and itself ruptured to form several very small satellite drops, while the majority of the filament settled out.

The lowest section of the fall column contained the equipment for measuring the fall velocity. Five 0.5-mV helium-neon lasers were spaced approximately 60 cm apart and aligned vertically and horizontally with a plumb line centered in the column. Their spacing was determined by hanging dimensionally stable aerial film in the column and exposing it to the lasers. In this manner, the vertical spacing could be measured to within ± 0.5 mm. The laser emission which was initially a 1-mm cylindrical beam was expanded by a double convex lens and then focused at the center of the column by a cylindrical lens into an ellipsoid of 5-mm major axis and 1-mm minor axis. Light was prevented from false scattering off the inner walls of the column by reception of the beam in a black box.

The basic technique of measurement is the detection of scattered light by the drop as it traverses the laser beam. Fiber optics, appropriately aligned, pick up and transmit the scattered light to a photomultiplier. The

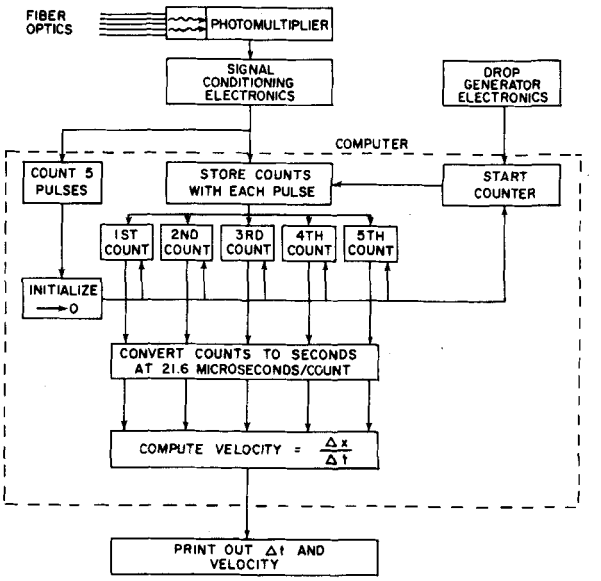

Figure 2. Signal processing and computer data reduction.

output of the photomultiplier is a spike of 0.1–0.5 V and typically 150 μs (microsecond) wide with a risetime of about 50 μs. These signals are easily handled by modern operational amplifiers in the signal conditioning electronics.

The signal conditioning electronics outputs a 5-V signal pulse directly to an interrupt input port of a Data General Micro Nova minicomputer. The flowchart of signal processing and computer data reduction is depicted in Figure 2. The computer has an internal counter which is initiated upon reception of a signal, denoting the production of a drop, from the drop generation electronics. As signals from the photomultiplier are received, the computer stores the countervalue in five successive registers. Thus, the difference of registers 1 and 2 represents the time between laser beams 1 and 2, the difference of registers 2 and 3, the time between laser beams 2 and 3, and so forth. Each count difference is converted to time at 21.6 μs per count. This scheme achieves a resolution of one part in two thousand or better and is extremely reproducible. The variation in velocity from drop to drop is essentially due only to variations in the drop mass.

DATA REDUCTION

Measurements of the fall velocity consist of a set of up to four time intervals resulting from a drop traversing through two or more lasers; i.e., traversing all five lasers gives four time intervals. Each time interval corresponds to a laser spacing interval. Data reduction then consists of calculating the terminal velocity from the set of measured velocities. Because of the differing behavior of large and small drops, the terminal velocity is computed differently for each size range.

In the range $100 < Re < 200$ measured, the drops reach terminal velocity in only a few meters. The drops are essentially spherical and do not oscillate; thus, once the drop stream is aligned with the laser beams, every drop successfully traverses all five lasers. There is no acceleration so that the terminal velocity is taken as the average of the four velocity intervals measured.

The larger drops ($Re > 800$) are known to be highly deformed and oscillate about their equilibrium shape; consequently, not all drops are able to successfully pass through all five laser beams. When a run was made with a given drop size of say 100 drops, perhaps one or two would successfully traverse all five lasers. Those measurements accepted were those in which at least three laser beams were hit. It turned out that the first laser was always hit, and in 98% of all accepted measurements at least four beams were hit. Although the lasers were nearly equally spaced, the extreme accuracy of the computer timing loop enabled one to determine which lasers were hit and which missed. Thus, if only three or four time intervals were measured, each interval could be properly identified corresponding to the appropriate space interval. The larger drops showed a slight acceleration in the computed velocity

TABLE 1. LIQUID PROPERTIES*

Liquid	ρ_l (kg/L)	μ(kg/m·s $\times 10^{-3}$)	σ(N/m $\times 10^{-3}$)	
Ethylene Glycol (EG)	1.106	19.90	48.40	
Propylene Glycol Isobutyl Ether (PiBT)	0.971	10.86	26.90	
Dipropylene Glycol Methyl Ether (DPM)	0.951	3.41	28.80	
Glycerol	1.253	300.0	63.00	
Newtonian Thickened DPM's				kg Elvacite/ L DPM
N1	0.953	3.94	~29.00	0.004
N2	0.953	5.04		0.020
N3	0.975	23.21		0.100
N4	1.020	453.00		0.175
N5	0.964	8.60		0.050
Non-Newtonian Thickened DPM's				kg K125/ L DPM
NN1	0.956	47.90	29.18	0.020
NN2	0.958	104.40		0.025
NN3	0.958	268.00	29.36	0.030
NN4	0.953	6.86		0.004
NN5	0.953	4.86		0.002

* The viscosity reported is the Ostwald viscosity. The surface tension was measured by the capillary rise technique. Note: 1 kg·m^{-1}·s^{-1} $\times 10^{-3}$ = 1 centipoise, and 1 N·m^{-1} $\times 10^{-3}$ = 1 dyne/cm.

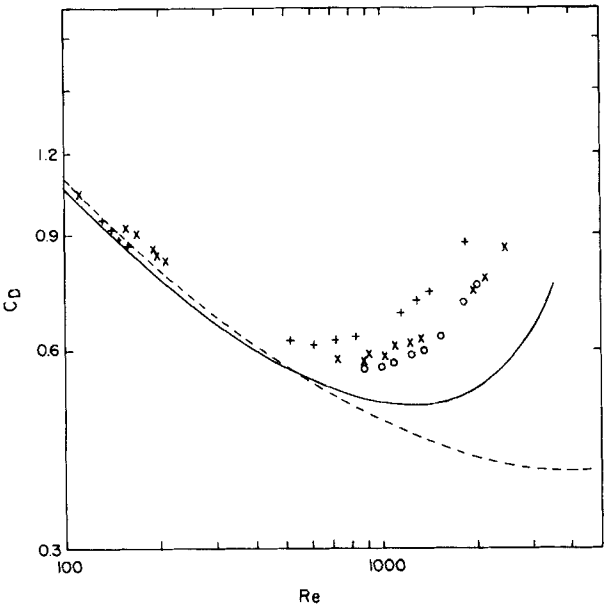

Figure 3. Reynolds number (Re) vs. drag coefficient (C_D). Solid line is for water (Gunn and Kinzer, 1949); dashed line for solid sphere (Davies, 1945): O-DPM, X-EG, +-PiBT (Table 1). Error limits are indicated by the size of the plotting symbols.

intervals. To compute the terminal velocity of a given drop size, all measurements of the same interval were averaged, the four resulting velocities were then fitted with an equation of the form

$$V = A \exp(-B/t). \tag{12}$$

It is evident that the terminal velocity is the coefficient A. In all cases the difference in the velocity of the last interval and the velocity of the first interval was $\leq 0.5\%$. The velocity of the last interval was always $\geq 99.5\%$ of the computed terminal velocity.

The scatter of the actual velocities as indicated by one standard deviation was typically 0.5% of the mean for a given velocity interval. Because of the measurement system used and its highly reproducible results, any calculations based on the measurements can be expected to be accurate and reliable. The Reynolds number and drag coefficient were computed from Eqs. 6 and 4, respectively.

RESULTS AND DISCUSSIONS

The primary result to be discussed is the effect of liquid viscosity on drag. It is not possible, however, to entirely neglect consideration of drop distortion since it acts concurrently with internal circulation. Without a great deal of mathematical analysis (Savic, 1951; McDonald, 1954; Pruppacher and Pitter, 1971), a proper consideration of surface tension and drop distortion is impossible. However, experimental measurements indicate substantially (Blanchard, 1949; Buzzard and Nedderman, 1967; Garner and Lihou, 1965) that decreasing surface tension increases drag because of the increased distortion. Neglecting for a moment the effects of viscosity, a liquid drop of lower surface tension than another should always exhibit a higher drag coefficient and approach asymptotically each other at lower Re (increasing sphericity). Thus, for example, two drag curves of liquids differing in surface tension can never cross. The discussion of viscosity effects that follows presumes that the above relation of surface tension to drag holds true.

These drag measurements cannot discern whether or not the internal circulation affects the drop shape significantly. Although the internal circulation alters the friction and pressure drag components, the relative magnitudes of the two possible physical mechanisms, drop distortion and surface liquid movement, which bring about the drag change cannot be ascertained. Previous computations of drop shape (Savic, 1950; Pruppacher and Pitter, 1971) have neglected internal circulation entirely and obtained deformations within the error of experiment. Most recently, Green (1975) has computed the axis ratio of deformed water drops considering only a balance of hydrostatic and surface tension forces at the equator of a drop. His results give an excellent fit to data obtained empirically. These investigations suggest that internal circulation does not affect the drop shape significantly.

A comment should be made concerning the possible effect of surface active material on the development of internal circulation. Since the liquid-gas systems under consideration are of very low viscosity ratio (μ_a/μ) at relatively high Re, the forces acting are not conducive to the formation of a concentration gradient of surface active material which would create a driving force opposing internal circulation (Marangoni effect) (Levich, 1962; Clift, 1978).

A first series of measurements were taken using three Newtonian liquids of differing surface tension and viscosity, Propylene Glycol Isobutyl Ether (PiBT), Ethylene Glycol (EG), and Dipropylene Glycol Methyl Ether (DPM). Their relevant physical properties are given in Table 1. The results of measurements, Figure 3, immediately indicate the importance of drop liquid viscosity affecting the drag via the internal circulation. The liquids PiBT and DPM are essentially of equal surface tension while only their viscosity differs yet PiBT's C_D is almost 20% greater (Re = 1,000). This is indicative of decreased internal circulation which acts via frictional drag and pressure drag. Reduced internal circulation increases shear at the drop surface and boundary layer separation occurs sooner resulting in a greater pressure drop in the wake. This general effect is also evidenced by the results of Buzzard and Nedderman (1967); however, the results reported here do not agree in two respects: first in the trend of the drag curve above Re = 1,000, secondly in the absolute values. Buzzard and Nedderman show a flattening of the C_D curve as $Re > 2{,}000$ and their silicone fluids of comparable surface tension and viscosity exhibit drag coefficients ~5–10% lower. Our results parallel the trend of the well-established C_D curve of water and our self-check measurements with water give terminal velocities with 1% agreement with Davies (1939, unpublished) reported in Best (1950) for an altitude of 1.5 km (5,000 ft) (ρ_a = 0.989 kg/L).

Measurements were taken at Re = 100–200 for PiBT and EG which show that the effect of internal circulation in reducing the drag is still significant at intermediate Re. The PiBt and EG curves cross at about Re = 500 although PiBT's surface tension should

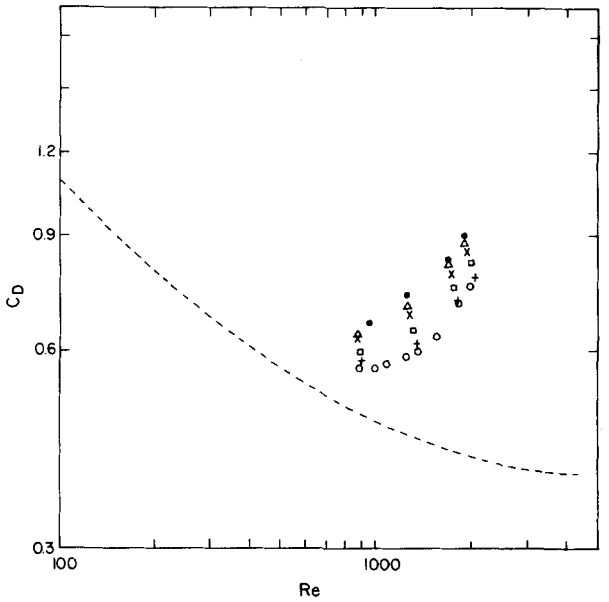

Figure 4. Reynolds number vs. drag coefficient for Newtonian thickened DPM: 0-3.41 m +-3.94, □-5.04, ×-8.60, △-23.21, ●-453, units are kg·m^{-1}·s^{-1} × 10^{-3}.

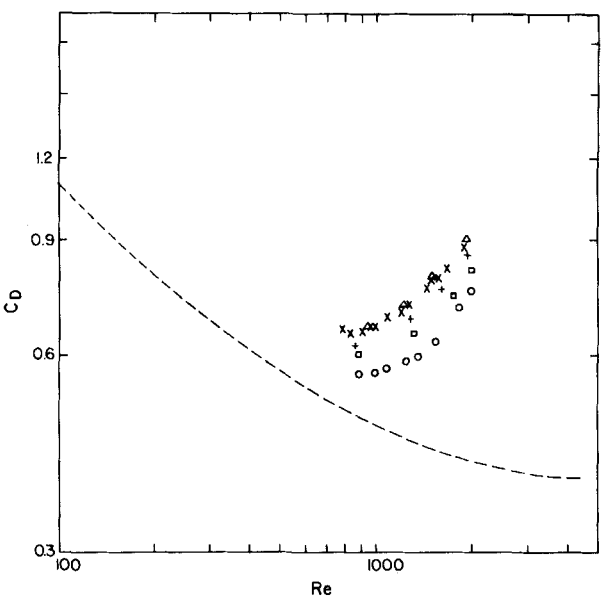

Figure 5. Reynolds number vs. drag coefficient for non-Newtonian thickened DPM: 0-3.41, □-4.86, +-6.86, ×-47.90, △-10.4, ●-268, units are kg·m^{-1}·s^{-1} × 10^{-3}.

place it above EG throughout the entire *Re* range. At this low *Re* range, the drops will be more closely spherical and the surface area in traction with the air is greater. Thus, the surface shear is more effective in transporting momentum to the internal fluid at lower *Re* due to the more spherical shape.

LeClair et al. (1972) calculate the velocity of the drop liquid at the surface and show that the internal circulation levels off for *Re* > 800. A limiting of internal circulation implies that drop distortion should eventually control the drag in the limit of higher *Re*. Our results corroborate this limiting of internal circulation. The curve of DPM becomes steeper than EG and crosses at *Re* ~ 1,800 so that the effect of drop distortion on drag predominates at higher *Re*. Greater distortion which acts to increase the pressure drag shifts the minimum of the drag curve to lower *Re*. The minimum can then be interpreted to represent the point at which drop distortion by decreasing the surface area available for traction and in conjunction with the flow pattern inhibits the transport of momentum to the drop liquid thereby limiting the internal circulation.

To quantitatively assess the effect of viscosity on drag, a series of measurements were taken in which the viscosity was changed while the surface tension was constant. For this task, DPM was thickened with two thickeners: 1. Elvacite (CH_2:C(CH_3)$COOCH_3$) an acrylic resin monomer; 2. Akryloid K-125, a methyl methacrylate resin polymer. DPM retains its Newtonian characteristics when thickened with Elvacite, whereas when thickened with Akryloid K-125 results in non-Newtonian properties. Chenier and Hill (1979) have measured the rheological properties of DPM thickened with K-125 extensively. They concluded that the addition of K-125 produced a non-Newtonian shear thinning solution that could be modeled by a power law over strain rates of 0.5 to 500 s^{-1}. For example, at a thickener concentration of 0.040 kg/L DPM (Ostwald viscosity = 0.514 kg·m^{-1}·s^{-1}) the power law relating shear stress (γ) to strain rate (ϵ) is

$$\gamma = (6.08 \pm 0.42)\epsilon(0.882 \pm 0.021) \tag{13}$$

The onset strain rate at which the viscosity decreases with increasing strain rate is 20 s^{-1} for a thickener concentration of only 0.020 kg/L DPM, (Ostwald viscosity = 0.046 kg·m^{-1}·s^{-}). Since thickener concentrations in this study exceed 0.020 kg/L DPM, the drag measurements should detect any difference of Newtonian vs. non-Newtonian liquid drops provided the strain rates exceed the onset strain rate. Unfortunately, strain rates for DPM drops are not known; however, strain rates for water drops can be obtained from the calculations of LeClair et al. (1970). The relevant component of the strain rate tension is given by (Middleman, 1968)

$$\epsilon_{r\theta} = \frac{1}{2}\left(\frac{1}{r}\frac{\partial u}{\theta} + \frac{\partial v}{\partial r} - \frac{v}{r}\right) \tag{14}$$

An analysis of Le Clair et al.'s graphical plot of the stream function (ψ) for *Re* = 300 at $\theta = 90°$ shows the radial velocity component to be very small. Only the angular component given by

$$v = \frac{1}{r\,sin}\left(\frac{\partial \psi}{\partial r}\right)_\theta \tag{15}$$

needs to be computed to evaluate $\epsilon_{r\theta}$. (In Le Clair et al. all variables are nondimensionalized. The nondimensional strain rate ($\epsilon'_{r\theta}$) is related to $\epsilon_{r\theta}$ by $E_{r\theta} = \epsilon_{r\theta}V_\infty/r$. For *Re* = 300, $V_\infty \sim 4.3$ m/s and r = 530 micron.) Crudeness in the estimate derives from the need to graphically read values of the radius corresponding to the stream function value. In the region between the vortex center and the drop surface, one calculates strain rates of approximately 1,000 s^{-1}. There is no direct way of using the strain rate for water to estimate a strain rate for a DPM drop; but, in view of such a high value as compared to the onset strain rate for non-Newtonian DPM, it strongly suggests that the actual strain rates in the DPM drops measured can be expected to exceed the onset strain rate. Thus, any differences in internal circulation between Newtonian and non-Newtonian DPM will be tested.

The results for Newtonian thickened DPM are shown in Figure 4 and non-Newtonian thickened DPM in Figure 5. Both show the decrease of drag with decrease of viscosity and show the paralleling of curves in this *Re* range. The plot of μ vs. C_D, Figure 6, shows that there is no difference between Newtonian and non-Newtonian fluids. A quantitative assessment of μ vs. C_D can be successfully approached by considering the mathematical functional form necessary to fit the eperimental data and exhibit appropriate limiting properties. The Stokes solution Eq. 11 strongly suggests that internal circulation is determined by the ratio μ_a/μ. The analysis of the proper mathematical function of μ_a/μ will now be considered.

Let us consider the functional relation

$$C_D = F\left(Re, \frac{\mu_a}{\mu}\right) \tag{16}$$

and assume

$$C_D = F(Re)F\left(\frac{\mu_a}{\mu}\right) \tag{17}$$

In the above relation, we are in effect assuming that the contributions of drop shape and internal circulation can be separated.

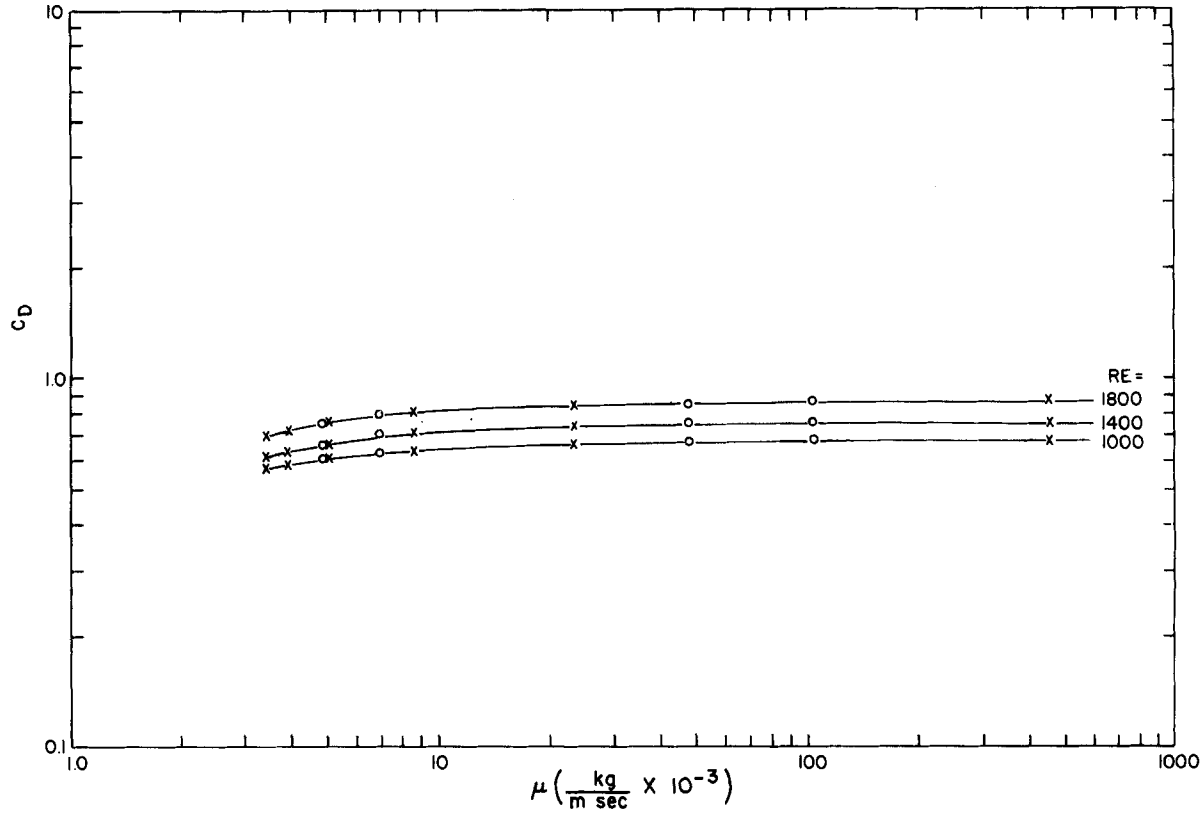

Figure 6. Viscosity (centipoises) vs. drag coefficient for Newtonian (×) and non-Newtonian (○) thickened DPM. Note: 1 centipoise = 1 kg·m^{-1}·s^{-1} × 10^{-3}.

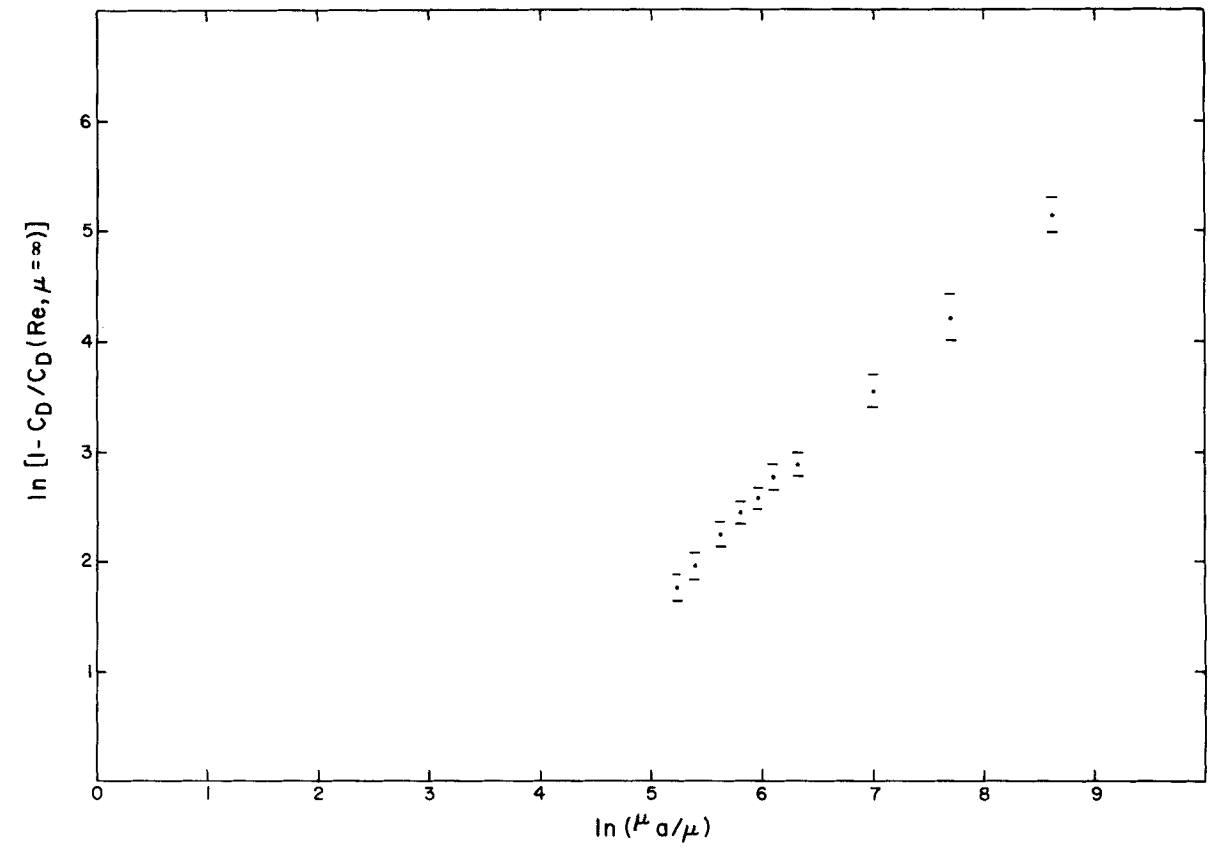

Figure 7. The relation of the viscosity ratio (μ_a/μ) to the viscosity function expressed by Eq. 2. Points plotted are derived from the *Re* = 1,000 curve of Figure 6.

The drop shape acts through $F(Re)$, since it may also contain an appropriate shape parameter. Calling $F(\mu_a/\mu)$ the viscosity function, a simple form such as

$$F\left(\frac{\mu_a}{\mu}\right) = 1 - B\left(\frac{\mu_a}{\mu}\right)^x, \tag{18}$$

can be considered. It also has the desirable limiting property

$$F\left(\frac{\mu_a}{\mu}\right) \to 1, \quad \frac{\mu_a}{\mu} \to 0. \tag{19}$$

We can then write

$$C_D = F(Re)\left[1 - B\left(\frac{\mu_a}{\mu}\right)^x\right] \tag{20}$$

but $F(Re)$ is just the drag coefficient for a noncirculating (infinite viscosity) deformable drop say C_D $(Re, \mu = \infty)$, which can be obtained from Figure 6. Subsequently, B and x can be found from

$$1 - \frac{C_D}{C_D(Re,\mu = \infty)} = B\left(\frac{\mu_a}{\mu}\right)^x \tag{21}$$

by least squares fit of the equation to data, Figure 7, for $Re = 1{,}000$ only. Equation 20 is reminiscent of Hadamard's (1911) solution for Stokes flow about a fluid sphere

$$C_D = C_{D_0}\left(1 - 1/3\,\frac{\mu_a}{\mu}\right). \tag{22}$$

The computed values are $x = 0.974$ and $B = 1/25.9$ at $Re = 1{,}000$ with a corelation of 0.99. The value of the exponent is strikingly close to 1.0, and it is not unreasonable to assume it should be $x = 1.0$. The form of Eq. 18 may very well be general; however, it is clear that the viscosity function cannot be entirely independent of Re all the way down to the Stokes region nor as $Re \to \infty$ since the drop shape changes significantly between these two extremes. The similarity of the Stokes flow solution to that for higher Re suggests the slightly more generalized viscosity function

$$F\left(Re, \frac{\mu_a}{\mu}\right) = 1 - B\,\frac{\mu_a}{\mu} f(Re) \tag{23}$$

Where $f(Re)$ would be some function of Re. For illustration only, if

$$C_D = C_D(Re,\mu = \infty)\left(1 - B\,\frac{\mu_a}{\mu} Re\right) \tag{24}$$

then $B = 1/30$ gives the Stokes flow solution at $Re = 10$ and excellent agreement with experimental data at $Re = 1{,}000$. To be definitive, however, requires measurements to extend the curves for DPM (Figures 4 and 5) down to the Stokes region.

If the viscosity function as expressed in Eq. 24 is tested against experimental data at higher Re (e.g., $Re = 1{,}800$), the linearity of μ_a/μ is preserved but the coefficient, B, must be adjusted smaller in order for Eq. 24 to be accurate. Thus, the functional dependence on Re is not properly expressed by a simple linear proportionality as expressed by Eq. 24.

ACKNOWLEDGMENTS

The authors would like to express their appreciation to: E. C. Penski, project monitor, for many helpful discussions; Donald Fielder and Louise Stunkard of Chemical Systems Laboratory, Aberdeen Proving Ground, for their measurement of the surface tension and viscosity of the liquids used: Bob Lape of Dow Chemical for supplying many of the chemicals used; and Bob Dalby and Larry Orcutt for their assistance in many of the experimental measurements.

This research was supported under contract number DAAG29-77-G-1072, U.S. Army Research Office.

NOTATION

A = numerical coefficient which equals V_T when $t = \infty$
B = numerical coefficient
C_D = coefficient of drag
C_{DF} = frictional component of C_D
C_{DP} = pressure component of C_D
C_{DS} = coefficient of drag for a solid sphere
C_{D_o} = coefficient of drag for Stokes flow
D = drag force on liquid drop
g = acceleration of gravity
m = mass of drop
Re = Reynolds number
r = radius of drop or radial position coordinate inside drop
u = radial velocity component of internal circulation
t = time
V = fall velocity of accelerating drop
V_T = terminal fall velocity of drop
V_∞ = velocity of flow field at an infinite distance from drop
v = angular velocity component of internal circulation
x = power law exponent

Greek Letters

ρ_a = density of air
ρ_l = density of liquid
μ_a = viscosity of air
μ = viscosity of liquid
γ = shearing stress
ϵ = strain rate
$\epsilon_{r\theta}$ = shear component of strain rate tensor
ψ = stream function of internal circulation
θ = angular position coordinate inside drop

LITERATURE CITED

Best, A. C., "Empirical formulae for the terminal velocity of water drops falling through the atmosphere," *Quart. J. Royal Meteor. Soc.*, **76**, 302 (1950).

Blanchard, D. C., "Experiments with water drops and the interaction between them at terminal velocity in air," Project Cirrus Occasional Rep., No. 17, General Electric Res. Lab., Schenectady (1949).

Buzzard, J. L., and R. M. Nedderman, "The drag coefficients of liquid droplets accelerating through air," *Chem. Eng. Sci.*, **22**, (1577).

Chenier, C. L., and G. A. Hill, "Physical properties of a thickened solven.. Suffield Technical Note," No. 435, Defense Res. Establishment Suffield, Ralston, Alberta, Canada (1979).

Clift, R., *Bubbles, Drops, and Particles*, Academic Press, New York, 171 (1978).

Davies, C. N., "Definitive equations for the fluid resistance of spheres," *Proc. Phys. Soc.*, **57**, 259 (1945).

Eaton, L. R., and T. E. Hoffer, "Experiments on droplets in free fall I: Terminal velocity and wall effects," *J. Applied Meteor.*, **9**, 269 (1970).

Garner, F. H., and D. A. Lihou, "Mass transfer to and from drops in gaseous streams," DECHEMA Monogr., **55**, 155 (1965).

Green, A. W., "An approximation for the shapes of large raindrops," *J. Applied Meteor.*, **14**, 1578 (1975).

Gunn, R., and G. D. Kinzer, "The terminal velocity of fall for water drops in stagnant air," *J. Meteor.*, **6**, 243 (1949).

Hadamard, J., "Movement permanent lent d'une sphere liquid et visqueuse dans un liquid visqueux," *Compt. Rend*, **152**, 1735 (1911).

Hamielec, A. E., T. W. Hoffman, and L. L. Ross, "Numerical solution of the Navier Stokes equations for flow past spheres," *A. E. Ch. E. J.*, **13**, 212 (1967).

Happel, J., and H. Brenner, *Low Reynolds Number Hydrodynamics*, Englewood Cliffs, NJ, Prentice-Hall (1965).

LeClair, B. P., A. E. Hamielec, and H. R. Pruppacher, "A numerical study of the drag on a sphere at low and intermediate Reynolds number," *J. Atmos. Sci.*, **27**, 308 (1970).

LeClair, B. P., A. E. Hamielec, H. R. Pruppacher, and W. D. Hall, "A theoretical and experimental study of the internal circulation in water drops falling at terminal velocity in air," *J. Atmos. Sci.*, **29**, 728 (1972).

Levich, V. G., *Physiochemical Hydrodynamics*. Prentice-Hall, Inc., Englewood Cliffs, NJ, 391, 404, 426 (1962).

McDonald, J. E., "The shape and aerodynamics of large raindrops," *J. Meteor.*, **11**, 478 (1954).

Middleman, S., *The Flow of High Polymers*, John Wiley & Sons, Inc., New York, 245 (1968).
Pruppacher, H. R., and R. L. Pitter, "A semi-empirical determination of the shape of cloud and rain drops," *J. Atmos. Sci.*, **28**, 86 (1971).
Reynolds, O., "An experimental investigation of the circumstances which determine whether the motion of water shall be direct or sinuous and of the law of resisance in parallel channels," *Trans. Royal Soc. of London*, **A174**, 935 (1883).
Rybczinski, W., Referred to in H. Lamb's *Hydrodynamics*, 1932, Cambridge University Press, 738.
Savic, P., "Circulation and distortion of liquid drops falling through a viscous medium," Nat'l Research Council, Canada Report NRC-MT-22, 50 (1953).
Stokes, G. G., "On the effect of the internal friction of fluids on the motion of pendulums," *Cambridge Phil. Trans.*, **9** (1851).

Manuscript received November 30, 1981; revision received May 3, and accepted May 28, 1982.

Plasma—Particle Momentum and Heat Transfer: Modelling and Measurements

Measurements were made of the two-dimensional flow and temperature field in a d.c. plasma jet under different operating conditions. The particle velocity and the in-flight particle temperature were also measured for narrow cuts of alumina powders, of mean particle diameters of 18, 23, 39 and 46 μm, injected in the jet. The results are compared with the predictions of a one-dimensional mathematical model. The measured and computed particle velocities are in good agreement. This is, however, not the case for the particle temperature where considerable differences are observed. An attempt is made to determine the parameters which are often unduly neglected in modelling work and to identify the areas where further work is needed.

M. VARDELLE, A. VARDELLE, P. FAUCHAIS
Université de Limoges, France
and
M. I. BOULOS
Université de Sherbrooke
Québec, Canada

SCOPE

One of the applications of thermal plasma technology that has gained a wide acceptance on an industrial scale is plasma spray-coating. Presently, plasma spray-coating is used in a number of areas of the aerospace and manufacturing industries for the deposition of refractory and erosion-resistant coatings. Other applications such as wear resistance and weather-protection coatings are getting increasing attention. In either case, the basic technique used involves the injection of the powdered coating material in the tail flame of a d.c. plasma jet. As the particles are entrained by the jet, they are accelerated to a relatively high velocity, heated up and molten in a very short time. The formed droplets are then projected towards the substrate to be coated. On impact, the droplets solidify almost instantly and adhere to the surface of the substrate.

The quality of the coating is found to depend to a large extend on the particle velocity prior to the impact and whether or not all the particles were completely molten. Improvement of the quality of the coating obtained necessitated an intense research effort directed towards the study of the flow and temperature fields in a d.c. plasma jet and the characterization of the particle trajectory, temperature history and gas-particle heat transfer under plasma conditions. A special attention has also been given to the mathematical modelling of such a relatively complex system.

This paper reports an experimental and theoretical study of the gas and particle dynamics under conditions typically used in plasma spray-coating. The work involved the measurement of the gas velocity and temperature in d.c. plasma jet under different operating conditions. Measurements were also made of particle velocity and in-flight particle temperature for alumina particles injected in the jet. The results are compared with the predictions of a mathematical model.

CONCLUSIONS AND SIGNIFICANCE

From a comparison of the obtained experimental measurements and the predictions of a relatively simple one-dimensional mathematical model, it can be seen that the proposed model is adequate for the calculation of the particle velocity in the jet. The model, however, is far from being satisfactory when it comes to the calculation of the temperature history of the particles. In fact, contrary to experimental evidence, the model gave rise to very fast heating-up rates and melting of the particles. The difference could be due to the fact that resistance to internal heat transfer in the particles was neglected. It also could result from other effects not accounted for in the model such as thermophorises or carrier gas cooling, which could influence the particle trajectory and prevent it from penetrating the hot core of the jet.

The principal contribution of this work lies in the fact that it is the first time a comprehensive set of measurements is reported of the plasma velocity and temperature fields as well as the particle velocity and its in-flight temperature. From a comparison of this data with the predictions of the mathematical model, an attempt is made to determine the parameters which were unduly neglected in the model and to identify the areas where further work is needed.

0001-1541-83-6722-0236-$2.00.